ACS APPLIED MATERIALS & INTERFACES

Research Article

www.acsami.org

Processing Follows Function: Pushing the Formation of Self-Assembled Monolayers to High-Throughput Compatible Time Scales

Milan Alt,[†,‡,§] Janusz Schinke,[‡,∥] Sabina Hillebrandt,[‡,⊥] Marc Hänsel,[‡,#] Gerardo Hernandez-Sosa,[†,‡,○] Norman Mechau,[†,‡] Tobias Glaser,[‡,⊥] Eric Mankel,[‡,#] Manuel Hamburger,[‡,⊗] Kaja Deing,[‡,§] Wolfram Jaegermann,[‡,#] Annemarie Pucci,[‡,⊥] Wolfgang Kowalsky,[‡,∥] Uli Lemmer,[†,‡,○] and Robert Lovrincic*[,‡,∥]

[†]Light Technology Institute, Karlsruhe Institute of Technology, Engesserstrasse 13, 76131 Karlsruhe, Germany

[‡]InnovationLab GmbH, Speyerer Str. 4, Heidelberg, Germany

[§]Merck KGaA, Mainzer Straße 41, 64579 Gernsheim, Darmstadt, Germany

[∥]Institut für Hochfrequenztechnik, Technische Universität Braunschweig, Schleinitzstr. 22, 38106 Braunschweig, Germany

[⊥]Kirchhoff-Institut für Physik and [⊗]Organisch-Chemisches Institut, Universität Heidelberg, Im Neuenheimer Feld 227, 69120 Heidelberg, Germany

[#]Institute of Materials Science, Technische Universität Darmstadt, Petersenstrasse 32, 64287 Darmstadt, Germany

[○]Institute of Microstructure Technology, Karlsruhe Institute of Technology, Hermann-von-Helmholtz-Platz 1, 76344 Eggenstein-Leopoldshafen, Germany

ABSTRACT: Self-assembled monolayers (SAMs) of organic molecules can be used to tune interface energetics and thereby improve charge carrier injection at metal−semiconductor contacts. We investigate the compatibility of SAM formation with high-throughput processing techniques. Therefore, we examine the quality of SAMs, in terms of work function shift and chemical composition as measured with photoelectron and infrared spectroscopy and in dependency on molecular exposure during SAM formation. The functionality of the SAMs is determined by the performance increase of organic field-effect transistors upon SAM treatment of the source/drain contacts. This combined analytical and device-based approach enables us to minimize the necessary formation times via an optimization of the deposition conditions. Our findings demonstrate that SAMs composed of partially fluorinated alkanethiols can be prepared in ambient atmosphere from ethanol solution using immersion times as short as 5 s and still exhibit almost full charge injection functionality if process parameters are chosen carefully. This renders solution-processed SAMs compatible with high-throughput solution-based deposition techniques.

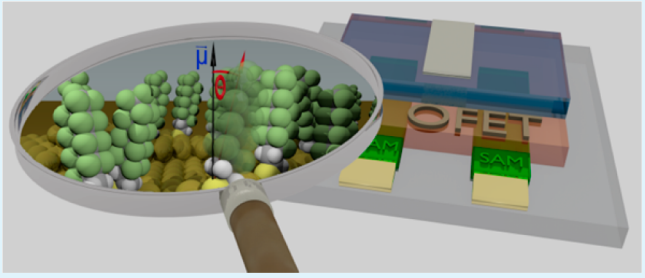

KEYWORDS: *self-assembled-monolayers, functional printing, organic electronics, organic field effect transistors, photoelectron spectroscopy, infrared spectroscopy*

INTRODUCTION

The great promise of organic electronics is based on the compatibility of organic materials with high-throughput, large-area, and cost-efficient processing techniques. However, one major obstacle on the route to fully solution processed devices is the limited availability of solution processable electrode materials. An important requirement for the optimal performance of all organic electronic devices (organic field-effect transistors (OFETs), organic solar cells (OPVs), organic light-emitting diodes (OLEDs), etc.) is that the frontier orbitals of the organic semiconductor are well-aligned with the corresponding electrode work function (WF) to reduce contact losses.[1] Injection layers can be used to tune the WF of the electrodes, facilitating the injection of charges into the lowest unoccupied molecular orbital (LUMO) or the highest occupied molecular orbital (HOMO) of the active material.

There are different approaches to alter the WF of an electrode, most importantly, by insertion of a transition metal oxide (TMO) layer,[2,3] a polymeric dipole layer (PDL),[4,5] or a self-assembled monolayer (SAM).[6,7] All these approaches possess different unique selling points. Advantages of SAMs are the ease of preparation, vast physiochemical and structural versatility, and a distinct final layer thickness. Moreover, SAMs can be structured laterally on various surfaces using different approaches,[8−10] prepared from single or multiple components,[8,11] and processed at room temperature, so that their deposition does not damage substrates with limited temperature tolerance.

Received: August 27, 2014
Accepted: October 17, 2014
Published: October 17, 2014

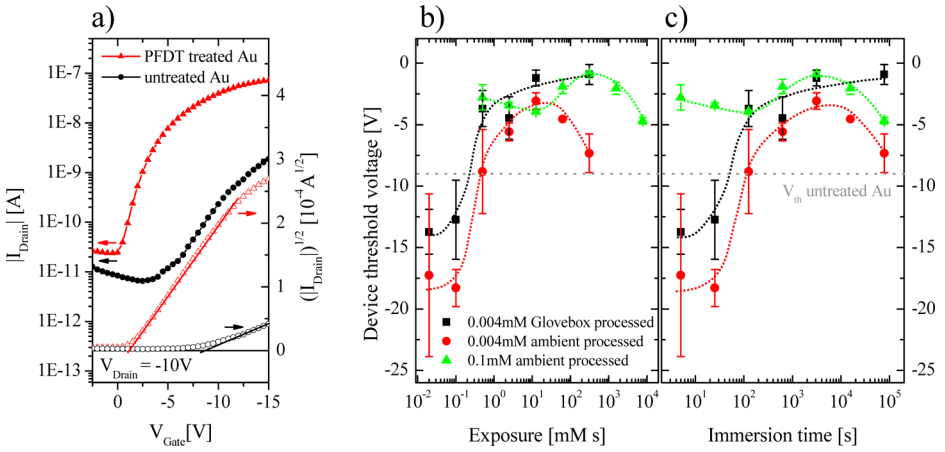

Figure 1. (a) Transfer characteristic of a typical OFETs with PFDT-treated and untreated Au contacts; (b) V_{th} of OFETs as a function of molecular exposure of the Au contacts to PFDT. (c) V_{th} of OFETs identical to (b) as a function of immersion time. The V_{th} values in (b) and (c) were averaged for at least four devices each with the standard deviation shown as statistical error. Lines connecting the data points are guide to the eyes.

SAMs have been a field of active research for more than three decades,[12,13] and over the past decade they have been successfully implemented as electrode modifiers in a multitude of organic electronic devices.[7,14,15] Next to charge injection, SAMs were demonstrated in a variety of possible applications, such as chemical sensing,[16,17] surface passivation,[18,19] or molecular devices.[20,21] Analytic studies on SAM quality and structure are, however, typically performed in highly controlled inert environment, using immersion of the substrate in very dilute solutions for several hours or even days. Although saturated coverage and ordering can be ensured this way, realistic application scenarios of SAMs with high-throughput deposition techniques require processability under ambient conditions and immersion times of a few seconds.

The accepted model for SAM formation differentiates between surface coverage and molecular orientation/ordering. While coverage, for example, for alkanethiols is completed within seconds,[22−25] initially in a "lying down phase",[26] the ordering process of the alkanethiol tails along each other can take hours or days, depending on the tail length and SAM process parameters.[27−29] In other words, these two growth phases occur on different time scales, one fast and potentially suitable for high-throughput processing, the other one time-consuming and most probably unsuited for such. It has been shown that phosphonic acid SAMs can be prepared on oxide surfaces with high quality and functionality via spin coating from nonpolar solvents, such as trichloroethylene and chloroform.[30−32]

Although there are numerous studies on thiol SAM accumulation on metal surfaces at short times, they focus on the SAM *quality*, such as coverage and ordering.[23,25,27,28,33] Studies on thiol SAMs as injection layers, however, are typically carried out on SAMs prepared with long (~24 h) immersion to ensure well-saturated SAMs.[7,14,34]

The motivation for this work is the investigation of the relationship between quality and functionality (i.e., improved charge injection) of SAMs, when deposited from solution under ambient conditions, and with immersion times relevant for high-throughput processes. We focus on the central question: How much quality is actually needed for satisfying functionality? We chose 1*H*,1*H*,2*H*,2*H*-perfluorodecanethiol (PFDT) immobilized on Au surfaces as model system, as partially fluorinated alkanethiols have been studied extensively and were demonstrated to be versatile for application in metal WF tuning.[35−39] PFDT is known to increase the WF of Au by ~0.5 eV.[40] We investigated the formation process of PFDT SAMs by varying the molecular exposure (defined as product of immersion time of the substrate and the concentration of the solution) and the processing environment. To compare functionality and quality, SAMs were characterized by X-ray- and UV-photoelectron spectroscopy (XPS/UPS) and IR-reflection−absorption-spectroscopy (IRRAS), and they were implemented as charge injection layers in OFETs.

Our findings demonstrate that exposure of Au surfaces with PFDT in solution leads to (i) a fully covered SAM layer with substantial injection functionality prepared with high concentration in ambient conditions as fast as 5 s and (ii) a fully covered and oriented SAM layer with full functionality for charge injection after an exposure of 10 s·mM in inert atmosphere. However, a decrease in charge injection functionality with long immersion under ambient conditions is induced by a chemical change of the PFDT monolayer.

RESULTS AND DISCUSSION

Organic Field Effect Transistor Devices. In Figure 1a OFET devices containing PFDT (chemical structure PFDT: Figure 2a) treated Au source-drain contacts are compared to devices with untreated Au contacts. A schematic cross section

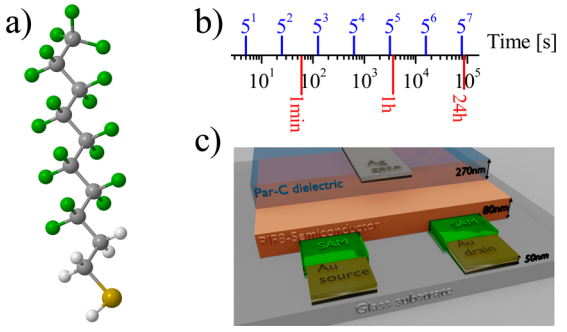

Figure 2. (a) Chemical structure of PFDT (white: hydrogen, yellow: sulfur, gray: carbon, green: fluorine) (b) Overview of prepared immersion times in logarithmic scale (blue) and time markers for orientation (red). (c) Schematic cross section of the bottom-contact top-gate OFET stack.

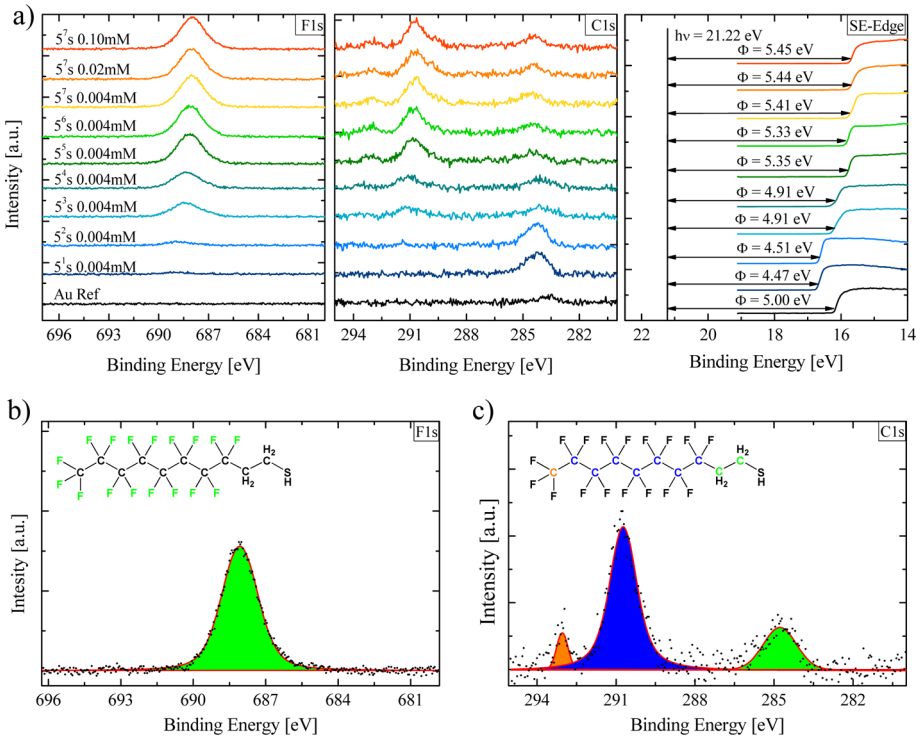

Figure 3. (a) XPS and UPS spectra. F 1s and C 1s emission and SE cutoff with and without SAM treatment, various immersion times, and different concentrations (0.004−0.1 mM). (b) Assignment of F 1s emission line to the molecular structure of PFDT. (c) Assignment of C 1s emission peaks to the molecular structure of PFDT. All data shown in this figure were derived from SAMs prepared under N_2 atmosphere in a glovebox. (b, c): Black dots correspond to the measured spectra but with background removed.

of the prepared devices is shown in Figure 2c. The PFDT-treated OFETs exhibit improved hole injection, reflected by a decreased threshold voltage (V_{th}). V_{th} was evaluated using the extrapolation in the saturation region (ESR) method as described in refs 33 and 34. The influence of the molecular concentration in solution, immersion time, and atmospheric condition on the charge injection functionality (i.e., V_{th}) of the SAM is presented in Figure 1b,c. In Figure 1b V_{th} is plotted as a function of exposure to the SAM molecules, defined by the product of immersion time and concentration. For very low exposure, the injection barrier was observed to increase with respect to the untreated Au contacts. As the coverage increases, the injection barrier decreases, and the best device performance is reached at an exposure of ∼10 s·mM. Comparing the behavior of the 0.1 mM and the 0.004 mM concentration series illustrates that the performance increase with SAM coverage is dominantly correlated to molecular exposure.

It is also observed that ambient-processed SAMs decrease in performance for high exposures. SAMs processed in N_2 atmosphere do not show this effect. This decrease in V_{th} under ambient conditions exhibits a correlation with immersion time, as shown in Figure 1c. In contrast to the initial change in performance increase driven by surface coverage, the final performance decrease is independent of the concentration. This suggests a fundamentally different effect to be responsible for the SAM functionality loss, such as a chemical reaction with the environment (e.g., oxidation). More details on the nature of this degradation effect will be presented later. Figure 1c also illustrates a significant reduction of V_{th} for SAMs that were immersed for 5 s in solution with 0.1 mM concentration. Although at this point the best SAM performance has not been reached yet, probably due to completed coverage but incomplete orientation of the molecules, it demonstrates that reasonable functioning SAMs can be accumulated as fast as 5 s. While highly appreciated for high-throughput application, such short dip coating times are experimentally difficult to control for a detailed study of the SAM formation. To observe SAM formation analytically under well-controlled experimental conditions, very low concentrations of 0.004 mM proved to be necessary for PFDT.

Photoelectron Spectroscopy. In Figure 3a the XPS core level emission lines for F 1s and C 1s and the secondary electron (SE) cutoff of SAM-covered Au surfaces are shown with increasing exposure to PFDT solution from bottom to top. Analogous to the OFETs discussed above, a series of samples immersed in 0.004 mM concentration for 5−5^7 seconds was prepared for XPS/UPS and IRRAS. Additionally, high-exposure SAMs using 5^7 s immersion in 0.02 mM and 0.1 mM were investigated. The F 1s emission line shows the increasing coverage of the PFDT monolayer with increasing immersion time until the monolayer formation is completed (after 5^6 s). The C1 emission line shows that a first carbon species for very low exposures (5 s, 5^2 s) is replaced by three different carbon species, which correspond to the chemical composition of the PFDT molecule (Figure 3b). We refer the initial carbon line to other adsorbates (possibly solvent molecules), which are gradually replaced by PFDT with increasing immersion time.

A consistent effect is observed in the SE cutoff plot, where initially a WF decrease can be observed. This phenomenon is known for noble metals as pillow effect[41−44] and does explain the inverse effect of low-exposure SAMs on V_{th} in OFETs discussed earlier. With advancing monolayer formation the WF shifts to higher values, exceeds the untreated Au reference at ∼5^3 s (2.5 s·mM), and saturates at approximately 5.45 eV.

dx.doi.org/10.1021/am5057689 | ACS Appl. Mater. Interfaces 2014, 6, 20234−20241

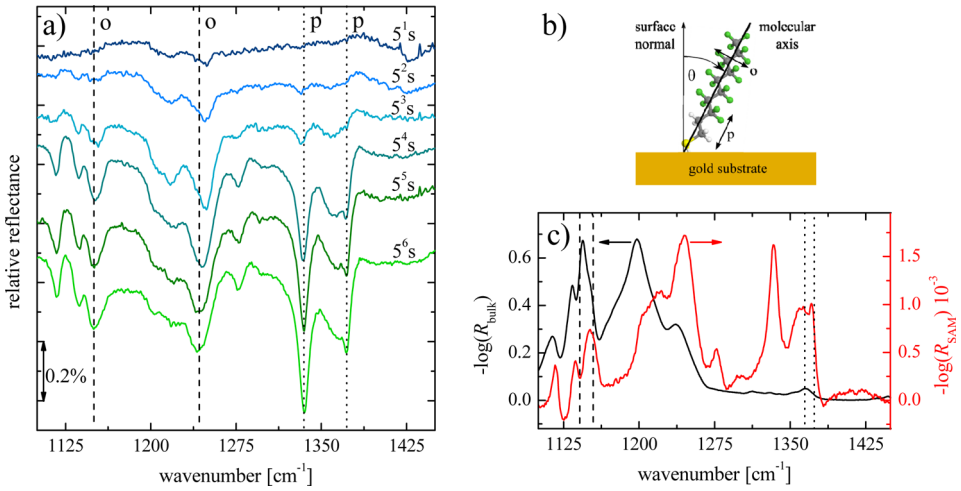

Figure 4. (a) IRRA spectra of PFDT monolayers for different immersion times of the gold substrate in a 0.004 mM solution. The dotted and dashed lines mark vibrational modes with the transition dipole moment parallel (p) and orthogonal (o), respectively, to the molecular axis according to Alves and Porter[47] and Pellerite et al.[50] (b) Schematic visualization of PFDT on the gold surface with tilt angle θ and orientation of vibrational modes. (c) Absorbance spectra of PFDT as a SAM (measured in IRRAS geometry) and as isotropic bulk (measured in ATR geometry). The dashed and dotted lines mark the used orthogonal and parallel modes at 1150 and 1370 cm^{-1}, respectively. All data shown in this figure were derived from SAMs prepared under N_2 atmosphere in a glovebox.

Infrared Reflection Absorption Spectroscopy. The infrared reflection absorption (IRRA) spectra in Figure 4a of PFDT SAMs (concentration 0.004 mM) clearly show strong changes with increasing immersion time in the absolute as well as relative intensities of the vibrational modes. Full spectra analysis reveals that the shortest immersion times (5 s, 5^2 s) exhibit peak features that cannot be assigned to vibrations of PFDT. This supports observations from OFET devices and PES discussed above, suggesting that the gold surface for such low exposures is covered with adsorbates. Because of the surface selection rule on metal surfaces only vibrational modes with a transition dipole moment component parallel to the surface normal can be excited with IRRAS. A PFDT molecule standing in a tilt angle θ relative to the surface normal is visualized in Figure 4b. Vibrational modes with the transition dipole moment orthogonal and parallel to the molecular axis are indicated by arrows. For short immersion times (5^3 s $\triangleq$ 0.5 s·mM) characteristic PFDT bands can be observed with the orthogonal bands showing a higher intensity than the parallel ones. With increasing immersion time, this ratio changes such that for long immersion times (5^6 s $\triangleq$ 62.5 s·mM) the parallel bands show the higher intensities indicating that the molecular axis is approaching the surface normal as expected in the SAM formation process.[29,45] The behavior correlates with the corresponding XPS measurements in Figure 3a showing strong changes between 5^2 s and 5^3 s. By quantification of the relative reflectance of the absorption bands with a transition dipole moment orthogonal ($R_{SAM,o}$) and parallel ($R_{SAM,p}$) to the molecular axis in the SAM and in the isotropic bulk ($R_{bulk,o}$ and $R_{bulk,p}$), we derived the tilt angle θ of PFDT for the different immersion times using the relation

$$\frac{\log(R_{SAM,p})}{\log(R_{SAM,o})}\cdot\left(\frac{\log(R_{bulk,p})}{\log(R_{bulk,o})}\right)^{-1}\cdot\frac{\nu_o}{\nu_p}=\frac{1}{\tan^2(\theta)}, \quad (1)$$

As the bulk measurements were performed in ATR geometry a dependence on the wavenumber ν_p and ν_o of the parallel and orthogonal absorption bands, respectively, must be considered within the term ν_o/ν_p. A comparison of the obtained bulk and SAM spectrum is shown in Figure 4c. The orthogonal and parallel modes that we used for the angle determination are marked. The derivation of the above equation is explained in the Experimental Section in more detail.

The final angle, in our case determined as 10(±3)°, also depends on various factors, including, for example, purity of the solvent, cleanliness, degradation, and roughness of the gold substrate.[45,46] Therefore, the slight deviation from reported literature values (12°−16°) can be explained.[47−49]

Comparison of Approaches. As demonstrated in the OFET section above, SAM formation initially is directly correlated to molecular exposure. To visualize the fast formation process, analytical studies were carried out using low concentration of 0.004 mM. In Figure 5, a comparison of resulting angle, WF, SAM coverage (measured by F 1s peak intensity), and threshold voltage of a series of SAMs prepared under inert atmosphere is shown. The three resulting data sets

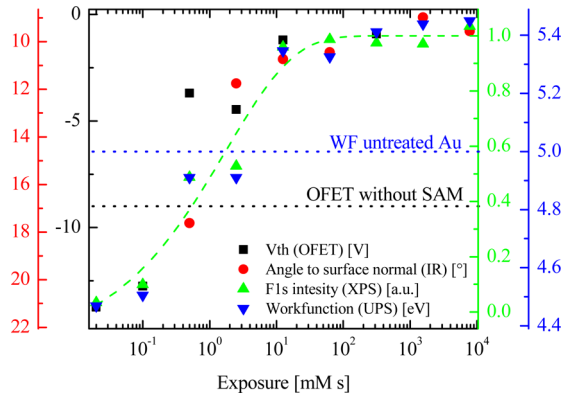

Figure 5. Compilation of measurements performed in this study. The F 1s emission, as indicator for surface coverage, is fitted to a Langmuir isotherm adsorption behavior (dashed green line). All data shown in this figure were derived from SAMs prepared using 0.004 mM concentration under N_2 atmosphere in a glovebox. The reference values of WF and threshold voltage of untreated samples are indicated by dotted lines.

dx.doi.org/10.1021/am5057689 | ACS Appl. Mater. Interfaces 2014, 6, 20234−20241

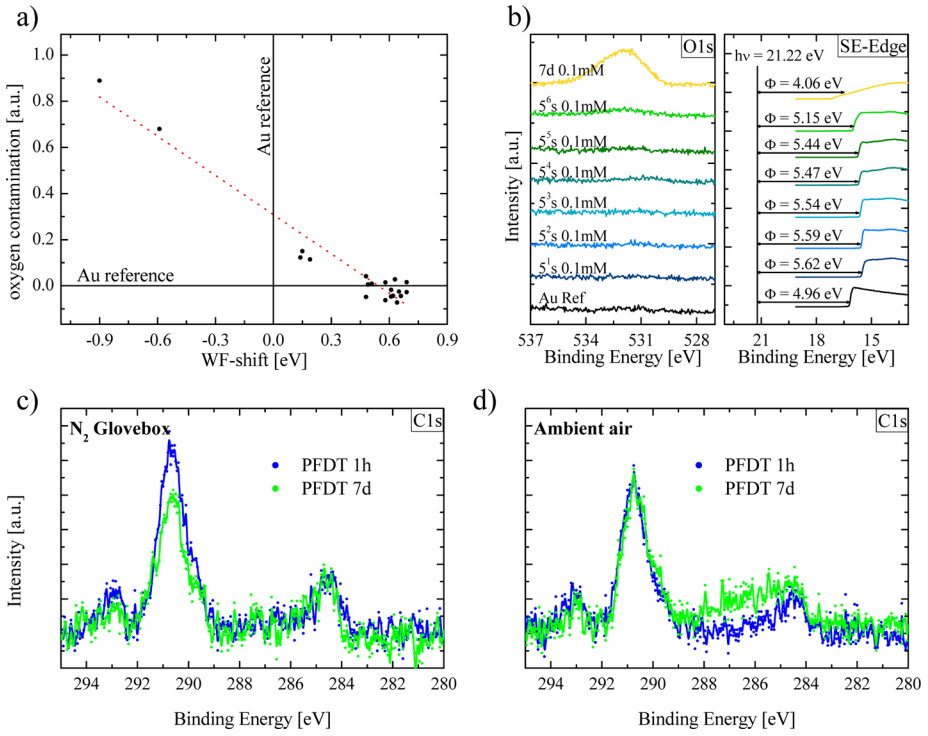

Figure 6. (a) oxygen contamination (as measured by integrated O 1s intensity) of ambient-processed SAMs against WF shift. (b) O 1s peak and respective WF shift measured by SE edge with PES (c, d) C 1s signal of SAMs prepared in a glovebox and under ambient condition. The dots correspond to the measured spectra but with background removed.

exhibit a similar behavior, indicating SAM formation to be completed at ~10 s·mM. With a concentration of 0.004 mM this refers to ~5^5 s immersion time.

Using a typical concentration of 0.1 mM yields a functional injection layer within seconds, as is demonstrated for ambient processed OFETs (Figure 1c).

Pellerite et al.[50] suggested a faster ordering process for partially fluorinated over nonfluorinated alkane tails, using phosphonic acid as anchor group on AlO_x surfaces. Although the nature of the binding group plays an important role in SAM formation, we assume the ordering process to be accelerated for thiol SAMs as well. This property renders molecules with partially fluorinated alkane tails as ideal candidates for SAM application with high-throughput processing techniques.

Ambient Processing of PFDT SAMS. In Figure 6a the WF shift (SE cutoff in the UPS spectra) of SAMs that were immersed in ambient atmosphere are plotted against their oxygen contamination, measured by the integrated PES oxygen signal intensity. The plot presents data from a wide range of immersion times, starting at a few seconds up to 7 weeks. Furthermore, a set of samples was prepared with higher concentration (0.1 mM) in ambient atmosphere. The O 1s and SE cutoff spectra are presented in Figure 6b. Using such a high concentration the maximum WF shift is achieved after only 5 s of immersion time. Clearly, there is a reverse linear correlation between the achieved WF shift and the oxygen contamination in the PFDT layer, not only canceling out the SAM functionality, but even resulting in a strong shift of 900 meV in the opposite direction. This is consistent with the SAM functionality loss in OFETs from exaggerated immersion time in ambient atmosphere presented above (Figure 1c). In Figure 6c,d the C 1s emission line of PFDT SAMs processed by immersion for 1 h and 7 d in different atmospheres is shown. When prepared in a N_2 glovebox (Figure 6c), the peak structure can be attributed to the three carbon species in the PFDT molecule for long and short immersion. When we compare the XPS spectra of samples processed under ambient conditions (Figure 6d), a slight change of the C 1s peaks at ~285 eV occurs between 1 h and 7 d immersion time. Therefore, we refer the loss in SAM functionality not to desorption of the SAM from the Au surface but rather to a change in the surface dipole due to partial oxidative degredation of the PFDT molecules. Oxidative degredation products of (partially) fluorinated hydrocarbons are well-studied in the context of their environmental hazard to the biosphere.[51,52] This is not an issue limited to PFDT alone, but to all fluorocarbon containing SAMs, like fluorobenzyl-mercaptans or fluorothiophenols.

Once the substrate with the SAM is removed from the ethanol solution and transferred into oxygen-free atmosphere or encapsulated by semiconductor and dielectric, no further decrease of the dipole of the molecule could be observed.

CONCLUSION

In summary, we demonstrated that PFDT SAMs, deposited by dip coating, can effectively shift the WF of Au surfaces by ~0.5 eV and enhance the hole injection into a p-type organic semiconductor within only a few seconds. The final average angle of PFDT molecules with respect to the surface normal was found by IR spectroscopy to be 10(±3) °. The V_{th} value of OFETs containing SAM-treated Au electrodes could be reduced by ~8 V to ~1 V with only 5 s immersion time.

We found that oxygen contaminations can counteract PFDT SAM functionality and even result in an opposing WF shift. This effect, however, is significant only after hours of immersion and therefore is not a fundamental restraint for printing partially fluorinated SAM injection layers, but it should

be considered for future investigations on SAMs as charge injection layers.

We conclude that deposition of such a SAM from ethanol in line with a high-throughput printing process is in principle possible. Crucial for successful application are process parameters that ensure on the one hand an exposure above the critical value concerning full coverage and on the other hand, if processed under ambient conditions, immersion times short enough to avoid oxidative degredation/contamination. The parameter to fulfill both of these prerequisites is molar concentration in the solution, which may be limited by a critical micellar concentration for some SAM-forming compounds.

EXPERIMENTAL SECTION

Sample Preparation. *SAM Deposition.* 1*H*,1*H*,2*H*,2*H*-Perfluorodecanethiol (PFDT, 97%, Sigma-Aldrich) and anhydrous ethanol (>99.8%, VWR) solvent were used as received. PFDT was handled in a glovebox and dissolved in ethanol at concentrations of 0.1, 0.02, and 0.004 mM, respectively. Ethanol containers were either freshly opened under the nitrogen atmosphere of a glovebox or in ambient in a fume hood and exposed to air for several hours to simulate realistic ambient oxygen contamination.

All samples used for the same concentration and time were immersed in the same thiol solution to maximize comparability. After a given time the samples were washed with pure ethanol, dried under nitrogen, and immediately transferred through ambient conditions to the respective measurement technique.

Analytic Samples. To exclude metal oxidation issues thin evaporated, polycrystalline gold films were used for the SAM formation. For IR and XPS samples silicon wafers with native oxide were used as substrates.

All substrates were cleaned with acetone and 2-propanol in an ultrasonic bath as well as treated with oxygen plasma before thermal evaporation. A thin (5 nm) titanium adhesion layer was deposited, followed by deposition of a 150 nm gold layer. The base pressure of the deposition chamber during evaporation was in the 10^{-6} mbar regime, the evaporation rate was approximately 2 Å/s. All substrates were then cleaned with argon plasma on both sides to remove organic contaminations without causing an oxidation of the gold layer. Further processing was carried out in two separated experiments: one sample preparation continued in nitrogen atmosphere and one in ambient atmosphere.

Devices. OFET devices were prepared in staggered bottom contact top gate (bctg) architecture on glass substrates. Glass substrates were cleaned with acetone and 2-propanol in an ultrasonic bath before thermal evaporation of 60 nm Au source-drain contacts via a shadow mask. All transistors presented in this study feature 50 μm channel length by 1000 μm width.

The p-type semiconductor PIF8-TAA[53] was spin-coated in a N_2-filled glovebox on top of the SAM-treated substrates from a 10 mL/mg chloroform solution and heated on a hot plate for 3 min at 100 °C, yielding ~75(±5) nm thick active layers with surface roughness < 1 nm as determined via profilometry and atomic force microscopy, respectively.

Parylene-C dielectric was prepared as a 250(+/10) nm thick layer on top of the active layer via vapor-phase deposition from a PDS2010 Coating System by SPS™.

Gate electrodes were prepared by thermal evaporation of 100 nm Ag via shadow mask structuring.

Characterization. *IRRAS.* IR-reflection−absorption spectroscopy (IRRAS) was performed using a Vertex 80v (Bruker) Fourier-transform (FT) IR spectrometer equipped with a liquid nitrogen-cooled MCT detector. The samples were positioned in a customized reflection unit inside the sample compartment of the spectrometer that was evacuated to about 3 mbar. The spectra were obtained using p-polarized light with an angle of incidence of 80° with respect to the surface normal. All spectra are the average of 500 scans with a resolution of 1 cm^{-1}. Each SAM measurement was divided by background spectrum of a clean gold substrate, thus giving the relative reflectance R of the monolayer.

In reflection geometry on metal substrates the intensity I of a vibrational mode is dependant on the orientation of the transition dipole moment $\vec{M}$ relative to the surface normal $\vec{z}$:[54]

$$I \propto |\vec{M}\cdot\vec{z}|^2 \propto \cos^2(\theta)$$

with the angle θ between the transition dipole moment and the surface normal.

The anisotropy of the molecules in the SAM compared to an isotropic bulk sample, different thicknesses d of the SAM and bulk, as well as an optical enhancement factor E_{op} of the gold surface led to the expression for the intensity ratios of one vibrational mode[48]

$$\frac{\log(R_{SAM})}{\log(R_{bulk})}\cdot\frac{d_{bulk}}{d_{SAM}}\cdot\frac{1}{E_{op}} = 3\cos^2(\theta)$$

The spectrum of the bulk material was acquired with an FT/IR 4000 spectrometer (Jasco) equipped with an ATR unit (GladiATR, PIKE-Technologies). The ATR spectrum is an average over 100 scans with a resolution of 1 cm^{-1}. Building the ratios of the absorbance of a parallel (1370 cm^{-1}) and an orthogonal (1150 cm^{-1}) mode of both the SAM and the bulk spectrum as shown in Figure 4c and dividing those ratios, the equation simplifies to

$$\frac{\log(R_{SAM,p})}{\log(R_{SAM,o})}\cdot\left(\frac{A_{bulk,p}}{A_{bulk,o}}\right)^{-1}\cdot\frac{\nu_o}{\nu_p} = \frac{\cos^2(\theta_p)}{\cos^2(\theta_o)}$$

The factor (ν_o/ν_p) accounts for the ATR geometry corrections as the penetration depth d_{bulk} of the IR beam depends in this case on the used wavenumber ν. The trigonometric relations $\theta_p = 90° - \theta_o$ and $\sin(\theta) = \cos(90° - \theta)$ thus lead to a final expression for the tilt angle $\theta = \theta_p$ of the molecular axis relative to the surface normal (see Figure 4b):

$$\frac{\log(R_{SAM,p})}{\log(R_{SAM,o})}\cdot\left(\frac{\log(R_{bulk,p})}{\log(R_{bulk,o})}\right)^{-1}\cdot\frac{\nu_o}{\nu_p} = \frac{1}{\tan^2(\theta)}$$

This approach assumes that the transition dipole moments of the analyzed modes are oriented perpendicular to each other.

XPS/UPS. The PES measurements were performed using the VERSAPROBE II of PHI. The base pressure of the chamber during all measurements was in the 10^{-10} mbar regime. The XPS spectra were measured with monochromatised Al Kα radiation (1486.6 eV), whereas the SE edge measurements were recorded with HeI radiation (21.22 eV) of a He discharge lamp and a 2.5 eV bias voltage. The binding energy is given with respect to the Fermi level edge of a metallic sample. To determine the exact core level binding energies all measured emission lines were fitted; thus, a mixed Gaussian−Lorentzian profile was applied after Shirley background subtraction. To get a detailed picture of the sample survey spectra, the following core levels were measured: F 1s, C 1s, O 1s, Au 4f, and S 2p.

OFET Devices. Characterization was carried out under ambient conditions in a three-probe setup using an Agilent 4155C Semiconductor Parameter Analyzer. Transfer characteristics were measured by operating OFETs in accumulation mode. V_{th} were evaluated using the extrapolation in the saturation region (ESR) method as described in refs 33 and 34 All V_{th} shown in this study are average values from at least four single devices, providing the standard deviation as statistical error.

AUTHOR INFORMATION

Corresponding Author

*E-mail: robert.lovrincic@tu-braunschweig.de.

Author Contributions

SAM layers for analytical studies were prepared and optimized by J.S. OFET devices were prepared and characterized by M.A. XPS/UPS measurements were performed and evaluated by

M.H. IRRAS measurements were performed and evaluated by S.H. The manuscript was written by M.A., J.S., and S.H., with contributions of all authors. All authors have given approval to the final version of the manuscript.

Notes

The authors declare no competing financial interest.

■ ACKNOWLEDGMENTS

The authors acknowledge financial support via the MORPHEUS project (FKZ: 13N11701-13N11706) of the Leading-Edge Cluster Forum Organic Electronics managed by InnovationLab GmbH within the High-Tech Strategy for Germany of the Federal Ministry of Education and Research.

■ ABBREVIATIONS

SAM, self-assembled monolayer
PFDT, 1*H*,1*H*,2*H*,2*H*-perfluorodecanethiol
WF, work function
HOMO, highest occupied molecular orbital
LUMO lowest unoccupied molecular orbital
OFET, organic field effect transistor
IRRAS, infrared reflection absorption spectroscopy
XPS, X-ray photoelectron spectroscopy
UPS, ultraviolet photoelectron spectroscopy
ATR, attenuated total reflection

■ REFERENCES

(1) Natali, D.; Caironi, M. Charge Injection in Solution-Processed Organic Field-Effect Transistors: Physics, Models and Characterization Methods. *Adv. Mater.* **2012**, *24*, 1357−1387.
(2) Tokito, S.; Noda, K.; Taga, Y. Metal Oxides as a Hole-Injecting Layer for an Organic Electroluminescent Device. *J. Phys. D: Appl. Phys.* **1996**, *29*, 2750−2753.
(3) Meyer, J.; Hamwi, S.; Kröger, M.; Kowalsky, W.; Riedl, T.; Kahn, A. Transition Metal Oxides for Organic Electronics: Energetics, Device Physics and Applications. *Adv. Mater.* **2012**, *24*, 5408−5427.
(4) Xiong, T.; Wang, F.; Qiao, X.; Ma, D. A Soluble Nonionic Surfactant as Electron Injection Material for High-Efficiency Inverted Bottom-Emission Organic Light Emitting Diodes. *Appl. Phys. Lett.* **2008**, *93*, 123310.
(5) Zhou, Y.; Fuentes-Hernandez, C.; Shim, J.; Meyer, J.; Giordano, A. J.; Li, H.; Winget, P.; Papadopoulos, T.; Cheun, H.; Kim, J.; et al. A Universal Method to Produce Low-Work Function Electrodes for Organic Electronics. *Science* **2012**, *336*, 327−332.
(6) Campbell, I. H.; Rubin, S.; Zawodzinski, T. A.; Kress, J. D.; Martin, R. L.; Smith, D. L.; Barashkov, N. N.; Ferraris, J. P. Controlling Schottky Energy Barriers in Organic Electronic Devices Using Self-Assembled Monolayers. *Phys. Rev. B* **1996**, *54*, R14321−R14324.
(7) De Boer, B.; Hadipour, a.; Mandoc, M. M.; van Woudenbergh, T.; Blom, P. W. M. Tuning of Metal Work Functions with Self-Assembled Monolayers. *Adv. Mater.* **2005**, *17*, 621−625.
(8) Smith, R. K.; Lewis, P. a; Weiss, P. S. Patterning Self-Assembled Monolayers. *Prog. Surf. Sci.* **2004**, *75*, 1−68.
(9) Shabtai, K.; Rubinstein, I.; Cohen, S. R.; Cohen, H. High-Resolution Lateral Differentiation Using a Macroscopic Probe: XPS of Organic Monolayers on Composite Au−SiO 2 Surfaces. *J. Am. Chem. Soc.* **2000**, *122*, 4959−4962.
(10) Rosso, M.; Giesbers, M.; Schroen, K.; Zuilhof, H. Controlled Oxidation, Biofunctionalization, and Patterning of Alkyl Monolayers on Silicon and Silicon Nitride Surfaces Using Plasma Treatment. *Langmuir* **2010**, *26*, 866−872.
(11) Brewer, N. J.; Leggett, G. J. Chemical Force Microscopy of Mixed Self-Assembled Monolayers of Alkanethiols on Gold: Evidence for Phase Separation. *Langmuir* **2004**, *20*, 4109−4115.
(12) Nuzzo, R. G.; Allara, D. L. Adsorption of Bifunctional Organic Disulfides on Gold Surfaces. *J. Am. Chem. Soc.* **1983**, *105*, 4481−4483.
(13) Ulman, A. *Self-Assembled Monolayers of Thiols;* Academic Press: Waltham, MA, 1998; Vol. *24*, p 278.
(14) Hamadani, B. H.; Corley, D. A.; Ciszek, J. W.; Tour, J. M.; Natelson, D. Controlling Charge Injection in Organic Field-Effect Transistors Using Self-Assembled Monolayers. *Nano Lett.* **2006**, *6*, 1303−1306.
(15) Yip, H.-L.; Hau, S. K.; Baek, N. S.; Ma, H.; Jen, A. K.-Y. Polymer Solar Cells That Use Self-Assembled-Monolayer- Modified ZnO/Metals as Cathodes. *Adv. Mater.* **2008**, *20*, 2376−2382.
(16) Trilling, A. K.; Beekwilder, J.; Zuilhof, H. Antibody Orientation on Biosensor Surfaces: A Minireview. *Analyst* **2013**, *138*, 1619−1627.
(17) Andringa, A.-M.; Spijkman, M.-J.; Smits, E. C. P.; Mathijssen, S. G. J.; Hal, P. A.; van Setayesh, S.; Willard, N. P.; Borshchev, O. V.; Ponomarenko, S. A.; Blom, P. W. M.; et al. Gas Sensing with Self-Assembled Monolayer Field-Effect Transistors. *Org. Electron.* **2010**, *11*, 895−898.
(18) Sieval, a. B.; Linke, R.; Zuilhof, H.; Sudhölter, E. J. R. High-Quality Alkyl Monolayers on Silicon Surfaces. *Adv. Mater.* **2000**, *12*, 1457−1460.
(19) Haj-Yahia, A.-E.; Yaffe, O.; Bendikov, T.; Cohen, H.; Feldman, Y.; Vilan, A.; Cahen, D. Substituent Variation Drives Metal/monolayer/semiconductor Junctions from Strongly Rectifying to Ohmic Behavior. *Adv. Mater.* **2013**, *25*, 702−706.
(20) Mantooth, B.; Weiss, P. Fabrication, Assembly, and Characterization of Molecular Electronic Components. *Proc. IEEE* **2003**, *9*, 1785−1802.
(21) Yu, X.; Lovrinčić, R.; Kraynis, O.; Man, G.; Ely, T.; Zohar, A.; Toledano, T.; Cahen, D.; Vilan, A. Fabrication of Reproducible, Integration-Compatible Hybrid Molecular/Si Electronics. *Small* **2014**, DOI: 10.1002/smll.201400484.
(22) Thomas, R. C.; Sun, L.; Crooks, R. M.; Ricco, A. J. Real-Time Measurements of the Gas-Phase Adsorption of N-Alkylthiol Mono- and Multilayers on Gold. *Langmuir* **1991**, *7*, 620−622.
(23) Karpovich, D.; Blanchard, G. Direct Measurement of the Adsorption Kinetics of Alkanethiolate Self-Assembled Monolayers on a Microcrystalline Gold Surface. *Langmuir* **1994**, 3315−3322.
(24) Kim, D. H.; Noh, J.; Hara, M.; Lee, H. An Adsorption Process Study on the Self-Assembled Monolayer Formation of Octadecanethiol Chemisorbed on Gold Surface. *Bull. Korean Chem. Soc.* **2001**, *22*, 276−280.
(25) Bensebaa, F.; Voicu, R.; Huron, L.; Ellis, T. H.; Kruus, E. Kinetics of Formation of Long-Chain N -Alkanethiolate Monolayers on Polycrystalline Gold. *Langmuir* **1997**, *13*, 5335−5340.
(26) Poirier, G.; Pylant, E. The Self-Assembly Mechanism of Alkanethiols on Au(111). *Science* **1996**, *272*, 1145−1148.
(27) Fruböse, C.; Doblhofer, K. In Situ Quartz-Microbalance Study of the Self-Assembly and Stability of Aliphatic Thiols on Polarized Gold Electrodes. *J. Chem. Soc., Faraday Trans.* **1995**, *91*, 1949.
(28) Bain, C. D.; Troughton, E. B.; Tao, Y. T.; Evall, J.; Whitesides, G. M.; Nuzzo, R. G. Formation of Monolayer Films by the Spontaneous Assembly of Organic Thiols from Solution onto Gold. *J. Am. Chem. Soc.* **1989**, *111*, 321−335.
(29) Poirier, G. E. Coverage-Dependent Phases and Phase Stability of Decanethiol on Au(111). *Langmuir* **1999**, *15*, 1167−1175.
(30) Nie, H.; Walzak, M. J.; McIntyre, N. S. Delivering Octadecylphosphonic Acid Self-Assembled Monolayers on a Si Wafer and Other Oxide Surfaces. *J. Phys. Chem. B* **2006**, *110*, 21101−21108.
(31) Acton, O.; Dubey, M.; Weidner, T.; O'Malley, K. M.; Kim, T.-W.; Ting, G. G.; Hutchins, D.; Baio, J. E.; Lovejoy, T. C.; Gage, A. H.; et al. Simultaneous Modification of Bottom-Contact Electrode and Dielectric Surfaces for Organic Thin-Film Transistors Through Single-Component Spin-Cast Monolayers. *Adv. Funct. Mater.* **2011**, *21*, 1476−1488.
(32) Cernetic, N.; Acton, O.; Weidner, T.; Hutchins, D. O.; Baio, J. E.; Ma, H.; Jen, A. K.-Y. Bottom-Contact Small-Molecule N-Type Organic Field Effect Transistors Achieved via Simultaneous Modification of Electrode and Dielectric Surfaces. *Org. Electron.* **2012**, *13*, 3226−3233.

(33) Rianasari, I.; Walder, L.; Burchardt, M.; Zawisza, I.; Wittstock, G. Inkjet-Printed Thiol Self-Assembled Monolayer Structures on Gold: Quality Control and Microarray Electrode Fabrication. *Langmuir* **2008**, *24*, 9110−9117.
(34) Bock, C.; Pham, D. V.; Kunze, U.; Käfer, D.; Witte, G.; Wöll, C. Improved Morphology and Charge Carrier Injection in Pentacene Field-Effect Transistors with Thiol-Treated Electrodes. *J. Appl. Phys.* **2006**, *100*, 114517.
(35) Frey, S.; Heister, K.; Zharnikov, M.; Grunze, M.; Tamada, K.; Coolorado, R.; Graupe, M.; Shmakova, O. E.; Lee, T. R. Structure of Self-Assembled Monolayers of Semifluorinated Alkanethiols on Gold and Silver Substrates. *Isr. J. Chem.* **2000**, *40*, 81−97.
(36) Alloway, D. M.; Hofmann, M.; Smith, D. L.; Gruhn, N. E.; Graham, A. L.; Colorado, R.; Wysocki, V. H.; Lee, T. R.; Lee, P. A.; Armstrong, N. R. Interface Dipoles Arising from Self-Assembled Monolayers on Gold: UV−Photoemission Studies of Alkanethiols and Partially Fluorinated Alkanethiols. *J. Phys. Chem. B* **2003**, *107*, 11690−11699.
(37) Shaporenko, A.; Cyganik, P.; Buck, M.; Ulman, A.; Zharnikov, M. Self-Assembled Monolayers of Semifluorinated Alkaneselenolates on Noble Metal Substrates. *Langmuir* **2005**, *21*, 8204−8213.
(38) Lu, H.; Zeysing, D.; Kind, M.; Terfort, A.; Zharnikov, M. Structure of Self-Assembled Monolayers of Partially Fluorinated Alkanethiols with a Fluorocarbon Part of Variable Length on Gold Substrate. *J. Phys. Chem. C* **2013**, *117*, 18967−18979.
(39) Venkataraman, N. V.; Zürcher, S.; Rossi, A.; Lee, S.; Naujoks, N.; Spencer, N. D. Spatial Tuning of the Metal Work Function by Means of Alkanethiol and Fluorinated Alkanethiol Gradients. *J. Phys. Chem. C* **2009**, *113*, 5620−5628.
(40) Tseng, C.-T.; Cheng, Y.-H.; Lee, M.-C. M.; Han, C.-C.; Cheng, C.-H.; Tao, Y.-T. Study of Anode Work Function Modified by Self-Assembled Monolayers on Pentacene/fullerene Organic Solar Cells. *Appl. Phys. Lett.* **2007**, *91*, 233510.
(41) Ishii, H.; Sugiyama, K.; Ito, E.; Seki, K. Energy Level Alignment and Interfacial Electronic Structures at Organic/Metal and Organic/Organic Interfaces. *Adv. Mater.* **1999**, *11*, 605−625.
(42) Bagus, P.; Staemmler, V.; Wöll, C. Exchangelike Effects for Closed-Shell Adsorbates: Interface Dipole and Work Function. *Phys. Rev. Lett.* **2002**, *89*, 096104.
(43) Kahn, A.; Koch, N.; Gao, W. Electronic Structure and Electrical Properties of Interfaces between Metals and Π-Conjugated Molecular Films. *J. Polym. Sci., Part B: Polym. Phys.* **2003**, *41*, 2529−2548.
(44) Hwang, J.; Wan, A.; Kahn, A. Energetics of Metal−organic Interfaces: New Experiments and Assessment of the Field. *Mater. Sci. Eng., R* **2009**, *64*, 1−31.
(45) Schwartz, D. K. Mechanisms and Kinetics of Self-Assembled Monolayer Formation. *Annu. Rev. Phys. Chem.* **2001**, *52*, 107−137.
(46) Käfer, D.; Ruppel, L.; Witte, G. Growth of Pentacene on Clean and Modified Gold Surfaces. *Phys. Rev. B* **2007**, *75*, 085309.
(47) Alves, C. A.; Porter, M. D. Atomic Force Microscopic Characterization of a Fluorinated Alkanethiolate Monolayer at Gold and Correlations to Electrochemical and Infrared Reflection Spectroscopic Structural Descriptions. *Langmuir* **1993**, *9*, 3507−3512.
(48) Chidsey, C. E. D.; Loiacono, D. N. Chemical Functionality in Self-Assembled Monolayers: Structural and Electrochemical Properties. *Langmuir* **1990**, *6*, 682−691.
(49) Liu, G.; Fenter, P.; Chidsey, C. E. D.; Ogletree, F.; Eisenberger, P.; Salmeron, M. An Unexpected Packing of Fluorinated N-Alkane Thiols on Au (111): A Combined Atomic Force Microscopy and X-Ray Diffraction Study. *J. Chem. Phys.* **1994**, *101*, 4301.
(50) Pellerite, M. J.; Dunbar, T. D.; Boardman, L. D.; Wood, E. J. Effects of Fluorination on Self-Assembled Monolayer Formation from Alkanephosphonic Acids on Aluminum: Kinetics and Structure. *J. Phys. Chem. B* **2003**, *107*, 11726−11736.
(51) Parsons, J.; Sáez, M.; Dolfing, J.; de Voogt, P. Biodegradation of Perfluorinated Compounds. In *Reviews of Environmental Contamination and Toxicology Vol 196 SE-2*; Whitacre, D. M., Ed.; Reviews of Environmental Contamination and Toxicology; Springer: New York, 2008; Vol. *196*, pp 53−71.
(52) Tsai, W.-T. An Overview of Environmental Hazards and Exposure Risk of Hydrofluorocarbons (HFCs). *Chemosphere* **2005**, *61*, 1539−1547.
(53) Zhang, W.; Smith, J.; Hamilton, R.; Heeney, M.; Kirkpatrick, J.; Song, K.; Watkins, S. E.; Anthopoulos, T.; McCulloch, I. Systematic Improvement in Charge Carrier Mobility of Air Stable Triarylamine Copolymers. *J. Am. Chem. Soc.* **2009**, *131*, 10814−10815.
(54) Allara, D. L.; Nuzzo, R. G. Spontaneously Organized Molecular Assemblies. 2. Quantitative Infrared Spectroscopic Determination of Equilibrium Structures of Solution-Adsorbed N-Alkanoic Acids on an Oxidized Aluminum Surface. *Langmuir* **1985**, *1*, 52−66.